Chemical Physics 176 (1993) 185–193
North-Holland

Photodetachment from laser-desorbed C_2^- ☆

Peter Wurz [1] **and Keith R. Lykke**
Materials Science/Chemistry Divisions, Argonne National Laboratory, 9700 S. Cass Avenue, Argonne, IL 60439, USA

Received 1 June 1993

We report on C_2^- desorption from graphite by pulsed laser light at 532 nm wavelength. The threshold fluence for laser desorption of C_2^- is 10 μJ/mm². For the first time, rotational analysis of a laser-desorbed negative molecular ion is performed. A rotational temperature of 1500 K is obtained by using two-photon resonance-enhanced detachment via the Herzberg–Lagerqvist band of C_2^-. This is in good agreement with our theoretical calculations for the surface heating during laser irradiation of graphite. Thermal desorption is identified as the responsible mechanism for particle removal at the low laser fluences probed in this study.

1. Introduction

Laser desorption of positive and negative ions from surfaces of various materials (electronic, organic, biomolecular, polymers, etc.) has become a widely accepted analytical tool for sensitive molecular characterization of surfaces and for identification of adsorbate species [1–3]. Therefore, a good understanding of the physical processes involved in the desorption of positive and negative ions is very desirable.

Desorption of particles by laser radiation of surfaces is observed at laser fluences above a certain threshold. Negative ions form more easily than their positive counterparts for carbon ions [4], a result reproduced recently [5]. We also found different thresholds for positive and negative ions, as well as for neutral molecules for the fullerenes [6]. From our work with organic materials, we conclude that a preference for the formation of negative ions over positive ions exists for many materials. For medium and high laser fluences, it is generally thought that the irradiating laser produces a plasma in front of the surface that is responsible for removal and ionization of sample material [4,5,7]. Thermal desorption processes have been considered for lower laser fluences, close to threshold fluence [6,8–10]. The graphite system is ideal for basic studies of laser desorption. It facilitates a well-defined and easily reproduced surface, and many of the molecules in the desorption spectra are well known from studies in the gas phase. A recent, comprehensive review on carbon molecules and their ions is given in ref. [11]. Some investigations of laser desorption from graphite samples have already been published for positive and negative ions [4,7] and for neutral molecules [9].

Our objective in this paper is to study the laser desorption of negative ions from graphite; apart from mass spectra [4,5], little else has been published thus far. Since C_2^- is one of the few negative ions that has a bound valence state below the continuum onset given by the electron affinity of 3.269 eV [12], it is a logical candidate for gaining further insight into the desorption process for negative ions. The spectroscopy of C_2^- is well known [13,14]. We use the electronic transition, $B\,^2\Sigma_u^+ \leftarrow X\,^2\Sigma_g^+$, discovered by Herzberg and Lagerqvist [13], for the determination of the rotational temperature. Later, Lineberger and Patterson proved that this transition was indeed caused by two-photon detachment from C_2^- [15]. We utilize this two-photon detachment to study the internal energy distribution for laser-desorbed negative ions. The $v'=0 \leftarrow v''=0$ vibrational transition is selected for its high Franck–Condon factor of 0.718 [14].

☆ Work supported by the US Department of Energy, BES-Materials Sciences, under Contract W-31-109-ENG-38.

[1] Present address: Physikalisches Institut, Universität Bern, Sidlerstrasse 5, 3012 Bern, Switzerland.

2. Experimental

The instrument used for these experiments is a laser desorption/laser ionization mass spectrometer. Most of the instrumental setup is identical to the one used previously [3,16]. Therefore, we discuss in detail only the present additions to the previous instrument that were necessary to accomplish these measurements. A schematic diagram of the current setup of the instrument is shown in fig. 1. The mass spectrometer is a linear time-of-flight (TOF) instrument of 120 cm length capable of recording desorbed negative and positive ions as well as neutral particles by means of an additional ionization laser. The graphite sample was sliced from a 1/2 inch rod (Bay Carbon) and polished. The top layers were then removed with an adhesive tape to obtain a clean surface before introduction into the vacuum chamber via the rapid sample exchange system.

The output of a pulsed (5 ns) frequency-doubled Q-switched Nd:YAG laser (532 nm) is split into two beams. One beam is directed through an adjustable attenuator and desorbs particles from the graphite sample (2×10^{-3} cm^2 spot size). The other part of the laser beam pumps a dye laser and is delayed appropriately to serve as the detachment laser pulse for the desorbed C_2^- molecule. The single-mode dye laser consists of an oscillator of the Littman type [17,18] and is amplified in four stages. We used fluorescein 548 as laser dye [19], which had a tuning range from $\approx$538 to $\approx$560 nm. A linewidth of less than 500 MHz is achieved with this system. Both laser beams enter the vacuum chamber through a LiF window. Before entering the vacuum system, the dye laser beam is focused with a cylindrical lens (FL 25 cm) to a line perpendicular to the ion path for higher detachment efficiency. The desorbed negative ions are accelerated up to $\approx$4 keV kinetic energy in one stage of 4

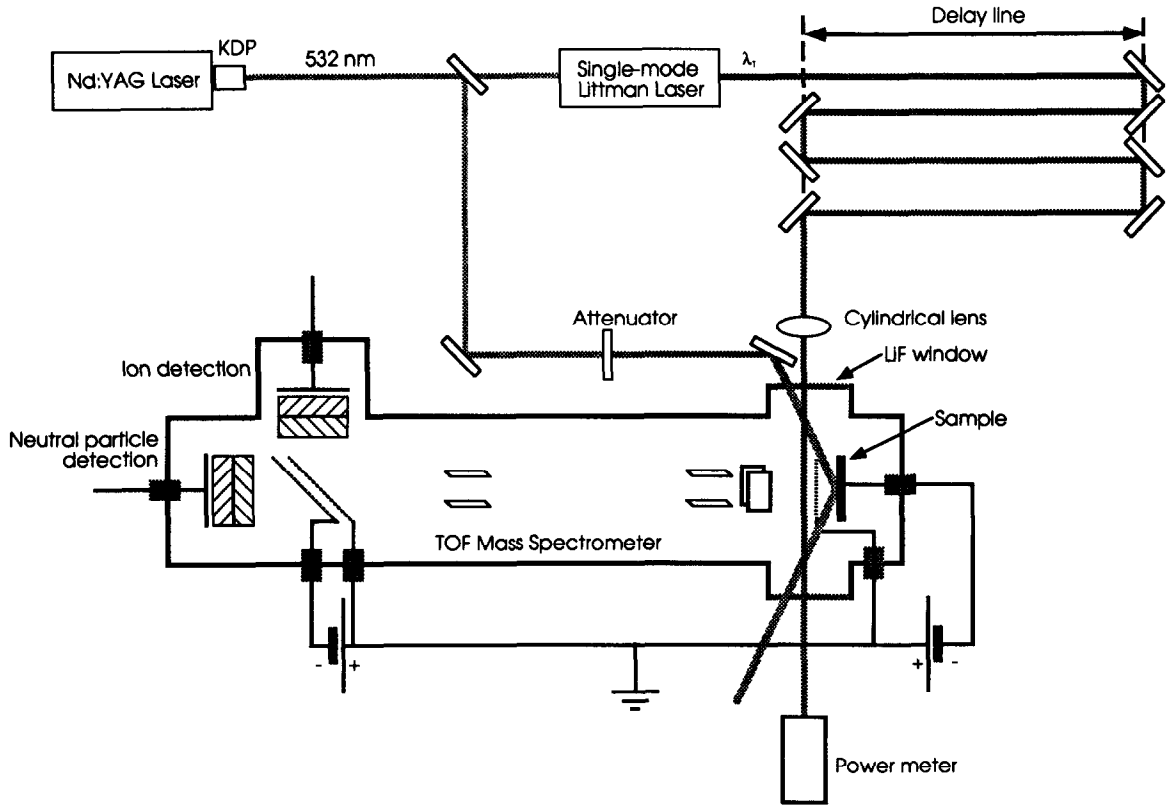

Fig. 1. Experimental setup of the time-of-flight instrument for the photodetachment measurements. The delay for the dye laser is set so that the C_2^- ion packet meets the dye laser pulse at 2 mm after the acceleration grid on the field-free drift path. Thus, ions and neutrals travel along at the same velocity until the ions are deflected to a separate ion detector by the reflector grids.

mm length before they enter the field-free TOF path. After 2 mm field-free flight, the ion beam is intersected by the detachment laser beam, which arrives ≈60 ns after the desorption laser beam. This is the calculated time it takes a C_2^- ion to travel from the desorption spot to the laser detachment region. A fraction of the ions become neutralized but still travel along with the ions to the end of the field-free path, since they have the same kinetic energy. The ions are separated from the neutral photodetached molecules by a set of two parallel grids. These grids have 92% geometrical transmission each. A total transmission of 42% is obtained at 45° incidence for the neutral as well as the ion channel. The negative ions are reflected at 90° off axis to the ion detector. The neutral molecules are undeflected and go straight through the grids to the neutral detector. Both detectors are dual microchannel plate assemblies in chevron configuration. The detector signal is acquired by a transient digitizer to obtain a mass spectrum and further processed electronically on a PC-based computer system. For the acquisition of the desorption threshold or detachment spectra, each of the detector signals is fed into a gated integrator with the gate (50 ns width) set at the C_2 and C_2^- peaks, respectively, and averaged for 30 times. The C_2^- signal is monitored to assure stable desorption signal conditions. Furthermore, the output power of the dye laser is recorded for the entire wavelength scan for calibration.

3. Results

Desorption of negative ions by laser irradiation of graphite is an efficient process. Fig. 2 shows a mass spectrum of the negative ions desorbed from graphite by 532 nm laser light. The lowest observed mass in the spectrum is the C_2^- molecular ion, and the spectrum extends to carbon cluster ions with sizes up to C_{12}^-. Every cluster size in between is observed, with C_4^- being the most abundant ion in the spectrum. The measured abundances are in good agreement with results obtained from laser desorption of carbon foils [4]. This is not surprising because the applied laser fluences are comparable: 30 μJ/mm² in our experiment and 52 μJ/mm² in their experiment. Since we have a linear TOF instrument with a short acceleration path, the carbon ions need to survive between 42 ns (for C^-) and 147 ns (for C_{12}^-) to be correctly identified. This is of particular interest for negative ions because they can lose an electron due to internal excitation [20], thus reducing detection efficiency or impairing mass identification.

The desorbed ion flux is, of course, strongly depen-

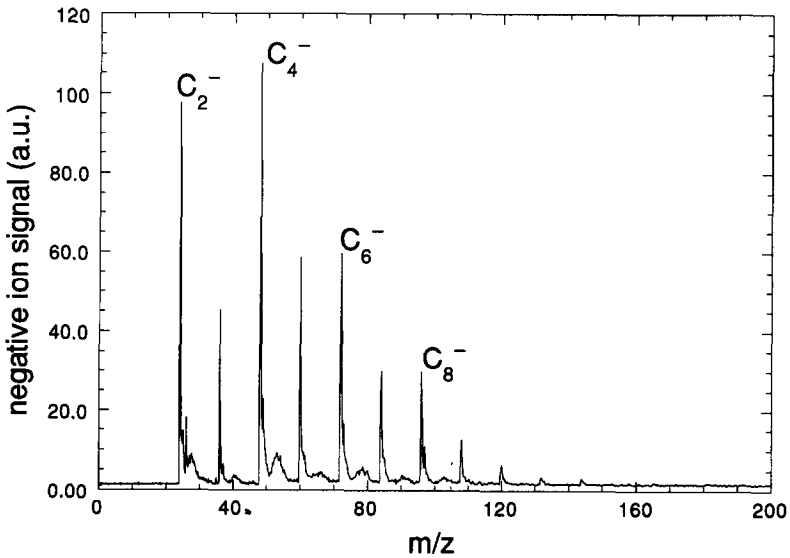

Fig. 2. Mass spectrum of the desorbed negative ions from graphite by 532 nm laser irradiation using a fluence of ≈30 μJ/mm². The ion detector was used for this measurement. The spectrum starts with C_2^-, and carbon molecules up to C_{12}^- can be identified.

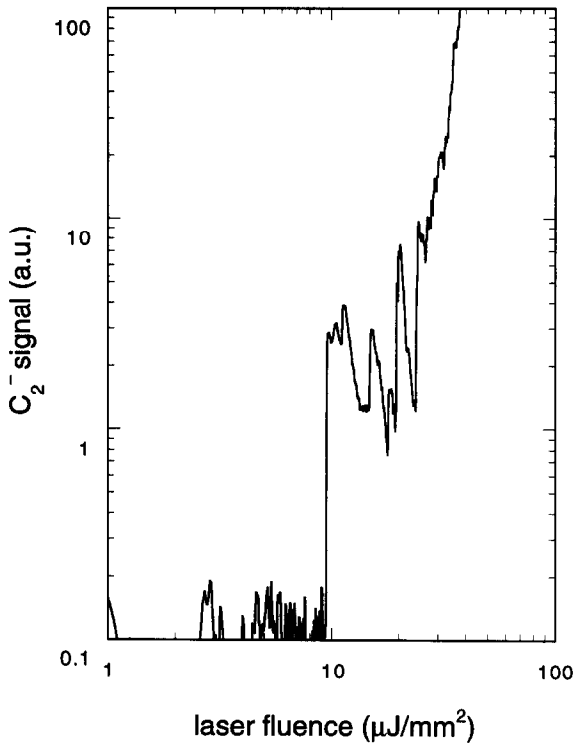

Fig. 3. Dependence of the C_2^- desorption signal on the irradiation power for 532 nm laser light. The apparent desorption threshold is at $\approx 10\ \mu J/mm^2$.

dent upon the fluence of the desorption laser. This dependence is shown in fig. 3 for the C_2^- ion. The apparent threshold fluence for desorption of C_2^- is $\approx 10\ \mu J/mm^2$. Above the threshold fluence, the signal rises sharply with increasing laser fluence. The observed structure above the threshold is of no significance because laser desorption is strongly dependent on the surface condition. We started with an unexposed graphite surface for the measurement shown in fig. 3. The laser fluence was increased continuously by the variable attenuator. After the threshold fluence is surpassed and desorption sets in, alteration and damage of the surface occur simultaneously [21]. This in turn changes the absorptivity of the surface and consequently the desorption flux, giving rise to the observed fluctuations in signal. Usually, the laser beam is rastered over the surface to avoid these signal fluctuations and to obtain a steady desorption signal. The irradiated area recovers after a few seconds and can be used for desorption again [6]. In the case of graphite, prolonged exposure of the irradiation site to the laser beam also provides stable desorption conditions. Therefore, we do not need to raster over the graphite surface. The laser fluence for these measurements was set to approximately three times the desorption threshold. The desorbed flux was monitored in real time by recording the C_2^- signal simultaneously. The ion channel always had much more signal than the neutral channel.

We used a (1+1) photon scheme with only one color for photodetachment of C_2^-. The first photon is resonant with the $B\,^2\Sigma_u^+$ level and a second photon of the same color detaches the electron from the molecular ion. In fig. 4, we show the measured photodetachment spectrum for C_2^- for the $B\,^2\Sigma_u^+ \leftarrow X\,^2\Sigma_g^+$ transition followed by nonresonant detachment. Unfortunately, the detection of the R branch is hindered by the declining efficiency of the laser dye towards shorter wavelengths. The displayed spectrum is a compromise between good signal/noise ratio and good resolution. The resolution is limited by power broadening since only one color was used for both bound–bound and bound–free transitions. The bound–free transition (detachment) has a much smaller cross section (by orders of magnitude) than the bound–bound transition. An improvement in resolution is expected for a two-color scheme, with a low fluence excitation laser for the resonant step and a high fluence ionization laser for the detachment of the electron. The laser for the resonant transition can

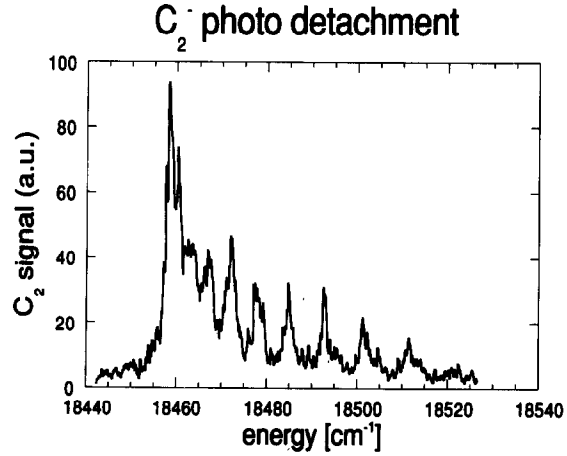

Fig. 4. Measured photodetachment spectrum for C_2^- for the (0, 0) band of the $B\,^2\Sigma_u^+ \leftarrow X\,^2\Sigma_g^+$ transition.

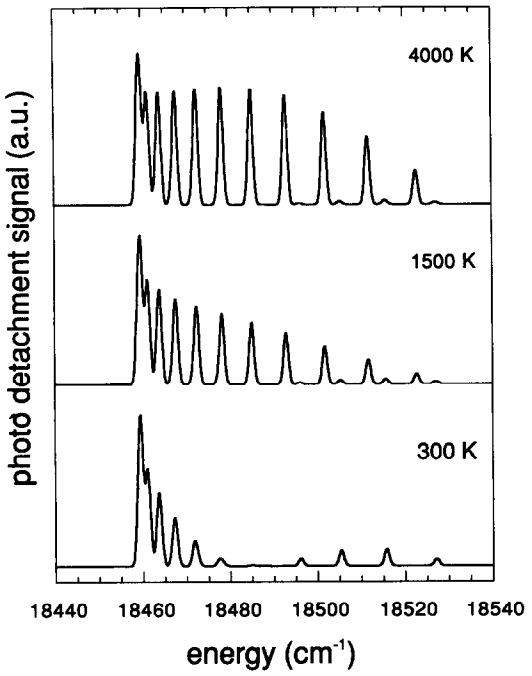

Fig. 5. Theoretical fit using a resolution of 1.2 cm^{-1} and temperatures of 300, 1500 and 4000 K. The efficiency of the dye laser, which decreases by ≈ 50% towards shorter wavelengths, has been folded into the calculation.

be of lower power and, therefore, enable measurements with higher resolution. Fig. 5 shows calculated spectra for temperatures of 300, 1500 and 4000 K. The various molecular constants that are used for the calculation are listed in table 1. The efficiency of the dye laser, which decreases by ≈ 50% towards shorter wavelengths, has been folded into the calculation. Good agreement with the measured data is achieved for 1500 K, considering the signal instabilities inherent in laser desorption.

Table 1
List of the molecular constants used for the calculation of the rotational spectrum of C_2^-, taken from refs. [14,22]

vibrational transition: $v'=0 \leftarrow v''=0$
Franck–Condon factor: 0.718
Hönl–London factors: $S_J^R = J'$, $S_J^P = J'+1$

$X\,^2\Sigma_g^+$ state:	$B\,^2\Sigma_u^+$ state:
$B_e = 1.7468$	$T_e = 18390.88$ cm^{-1}
$\alpha_e = 0.0167$	$B_e = 1.8774$
$\gamma_e = 0.$	$\alpha_e = 0.017$
	$\gamma_e = -0.00037$

4. Discussion

The rotational energy distribution for the laser-desorbed C_2^- ions yields a thermal distribution. This strongly suggests that the production of negative ions is due to a thermal desorption mechanism. Velocity distributions for large carbon molecules that were taken at very similar desorption conditions in this instrument also favor a thermal mechanism for desorption [6]. Of course, if we increase the fluence of the desorption laser substantially, the formation of a plasma plume in front of the surface is observed, as evidenced by enormous broadening of the peaks in the mass spectrum. This observation is in agreement with a recent report where, at higher laser fluences, a plasma that formed in front of the surface was found to be responsible for the generation of positive carbon ions [7].

The heating of a surface by a laser pulse can be calculated by evaluating the following equation [23]:

$$T(t) = \frac{\epsilon}{(\pi\kappa c)^{1/2}} \int_0^t \tau^{-1/2} R(t-\tau)\, \mathrm{d}\tau + T(0)\,, \qquad (1)$$

with κ the thermal conductivity, c the heat capacity, and ϵ the optical absorptivity of the surface. $R(t)$ is the laser pulse where we assumed a Gaussian temporal laser profile.

$$T(t) = \frac{\epsilon F}{\pi\sigma(2\kappa c)^{1/2}} \times \int_0^t \tau^{-1/2} \exp\left[-\frac{1}{2}\left(\frac{t-\tau-t_0}{\sigma}\right)^2\right] \mathrm{d}\tau + T(0)\,, \qquad (2)$$

with t_0 the time where the laser pulse peaks, $2(2\ln 2)^{1/2}\,\sigma = 5$ ns the fwhm of the laser pulse, and F the laser fluence. With the substitution $\sigma u = \tau + t_0 - t$, we get

$$T(t) = \frac{\epsilon F}{\pi(2\sigma\kappa c)^{1/2}} I(t/\sigma) + T(0) \qquad (3)$$

and

$$I(t/\sigma) = \int_{a-t/\sigma}^{a} (u+t/\sigma-a)^{-1/2}\exp[-(1/2)u^2]\,\mathrm{d}u\,, \tag{4}$$

where $a=t_0/\sigma$. For $a=6$ most of the Gaussian pulse is included in the integral. In eqs. (3) and (4), all the experimental parameters are in the preintegral factor and $I(t/\sigma)$ is of a general form. The calculation is done numerically and the result is depicted in fig. 6. For the determination of the peak temperature, we calculate the maximum of $I(t/\sigma)$ by setting $\mathrm{d}/\mathrm{d}t\,I(t'/\sigma)=0$, the integral peaks at $t'=t_0+\sigma$, with $I(t'/\sigma=(\frac{3}{2})^2$. Thus, the maximum temperature can be calculated by

$$T_{\max} = \frac{\epsilon F}{\pi(2\sigma\kappa c)^{1/2}}(\tfrac{3}{2})^2 + T(0)\,, \tag{5}$$

which gives approximately 2000 K in our case. The peak temperature scales linearly with the laser fluence and inversely with the square root of the pulse width. The calculated temperature fits well with our experimental observations considering that the measured temperature has contributions from the entire temperature profile. The tail of the temperature profile decays slowly to the initial temperature of the surface (≈ 100 μs), thus annealing the irradiated part of the surface.

For the investigated laser fluences, the number of hard-sphere collisions per particle is small enough that the rotational and vibrational distribution of the desorbed particles should not be altered noticeably. Thus, the internal temperatures approximately reflect the surface temperature during desorption. A Knudson layer, where the desorbed particles undergo numerous collisions in front of the surface, forms only at higher desorption rates and mainly affects the observed velocity distribution of the desorbed particles [24]. For graphite, the laser fluences where collisions start to influence the measured velocity distributions of C_2 were found to be above 6 mJ/mm^2; however, the internal energy distributions of C_2 remained largely unaffected [9]. Another process that could affect the rotational temperature of the negative cluster ions is dissociative electron attachment [25]. Due to the nature of dissociation, a considerable change in angular momentum can result. However, the high dissociation barrier to products of these small carbon clusters of ≈ 5–8 eV [26] and the short observation times in our experiment (on the order of 100 ns) will make it very unlikely to observe any influence from dissociative electron attachment.

The formation of negative ions is caused by elec-

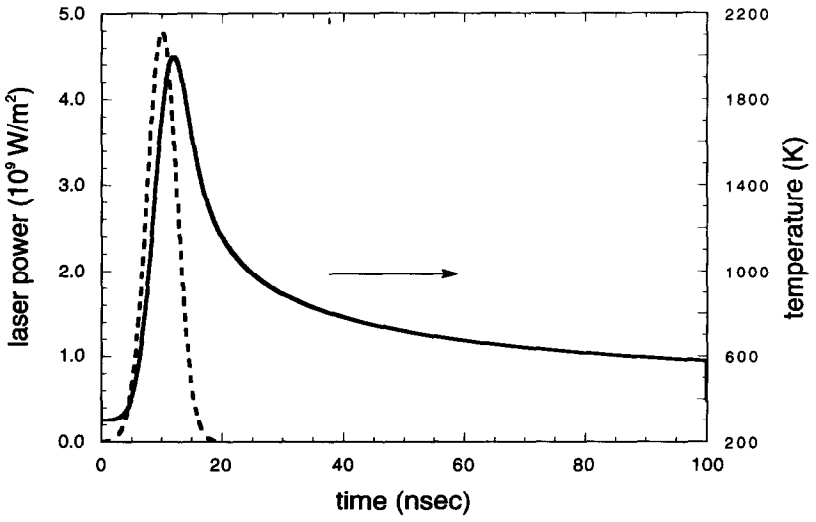

Fig. 6. Calculated surface temperature for heating graphite with a laser pulse of 30 μJ/mm^2. For the graphite surface, we used $\kappa=8.2$ W m^{-1} K^{-1} for the thermal conductivity, $c=0.45$ cal kg^{-1} K^{-1} for the heat capacity, and $\epsilon=0.95$ for the optical absorptivity. The dashed line shows the temporal profile of the laser pulse.

tron attachment to neutral molecules evaporated from the surface during the laser pulse. For the most part, the electrons are released from the surface by thermionic electron emission. Multiphoton effects, as suggested by Cronberg et al. [7], are negligible at our laser fluences. Strong experimental support for multiphoton effects has been reported recently [27], for laser powers orders of magnitude higher than used in our measurements. An extensive theoretical discussion of electron emission of laser heated surfaces is given by Lin and George [28], where electron emission is described by the generalized Richardson equation. For low laser powers, the generalized Richardson equation simplifies to the well-known Richardson–Dushman equation [29] for thermionic electron emission,

$$J(T) = ACT^2 \exp(-WF/k_B T) , \quad (6)$$

where $J(T)$ is the current, C is the "universal constant", A the electron emitting area, k_B the Boltzmann constant, and T the absolute temperature. For graphite, the thermionic work function $WF = 4.62$ eV and the universal constant $C = 60$ A cm^{-2} K^{-2} [30,31]. At 2000 K, this gives an electron emission rate of 3.38×10^{15} cm^{-2} s^{-1}. The observed negative ion mass spectrum is a convolution of evaporation of neutral molecules from the sample surface with the probability of ionization by electron attachment. Combining the thermionic electron emission with the electron attachment cross-section yields the probability p^- for formation of negative ions with an electron affinity of E_A

$$p^- = k \exp[(E_A - WF)/k_B T] . \quad (7)$$

With the factor $k = w(X^-)/w(X)$, the ratio of statistical weights for the negative ion and neutral molecule, eq. 7 is the well-known Saha–Langmuir equation for negative ion formation from hot surfaces [32]. For C_2, we obtain about 70 negative ions per laser shot, which is in good agreement with our experiment, taking into account the transmission of the instrument and the detection efficiency of the microchannel plates. A detailed derivation and discussion will be given in a forthcoming publication. The electron affinities for C^- to C_{12}^- are listed in table 2. The correlation between electron affinity and negative ion yield is easily seen from fig. 2. An additional influence to the observed negative ion abundances may arise from photodetachment by the desorption laser. At a wavelength of 532 nm, which corresponds to 2.33 eV, the signals for C^-, C_3^-, and C_{10}^- will be somewhat reduced.

The different electron affinities and ionization potentials for different molecules (see table 2) explain the relative abundances of negative and positive carbon molecular ions in the mass spectra [4,5]. Fur-

Table 2
Electron affinities [11,12,33,34], ionization potentials [35], partial pressures [36,37], and enthalpy of formation for the observed carbon molecules [36]

Cluster size C_n	Electron affinity (eV)	Ionization potential (eV)		Heat of sublimation (eV)	Partial pressure at 2000 K (Torr)	Particle flux (cm^{-2} s^{-1})
		theory	exp.			
1	1.27	11.0	11.27	7.35	3.35×10^{-8}	7.74×10^{12}
2	3.269	12.1	12.15	8.54	2.53×10^{-9}	4.14×10^{11}
3	1.95	11.2	12.6	8.64	3.95×10^{-8}	5.27×10^{12}
4	3.70	10.5		9.30	4.92×10^{-12}	5.69×10^{8}
5	2.80	10.7		10.7	3.8×10^{-12}	3.93×10^{8}
6	4.10	9.8	9.6	13.0	8.95×10^{-16}	8.44×10^{4}
7	3.10	10.0	8.09	13.8	1.64×10^{-16}	1.43×10^{4}
8	4.42	9.2	8.76			
9	3.70	9.4	8.76			
10	2.30		9.08			
11	4.00		7.45			
12	2.55		8.50			

thermore, this also explains the different experimental thresholds for negative and positive ions and neutral molecules [6]. Because the ions start out as neutral molecules, additional energy has to be expended for their formation. (Actually, negative ions lie lower than neutral atoms, so no extra energy is required. However, extra electrons are needed and this is the bottleneck for negative ion formation.) The threshold for the desorption of neutral molecules is the lowest because only the heat of sublimation has to be expended.

In thermal desorption, the desorbed flux depends exponentially on the surface temperature [38]. In addition, thermionic electron emission also depends exponentially on the surface temperature. Hence, a strong dependence on the temperature, and thus on the laser power, is obtained which establishes a laser desorption threshold by the sensitivity of the employed instrument. The desorption threshold we find for C_2^- in this study is much lower than was reported previously for desorption of C_2^+ ions by Cronberg et al. [7] and can be attributed to a much lower detection efficiency of their quadrupole mass spectrometer-based instrument.

5. Conclusions

In this experiment, we have demonstrated that a mass spectrometer with sufficient sensitivity allows photodetachment spectroscopy of negative ions in the thermal desorption regime, close to desorption threshold. By using a resonant two-photon scheme for photodetachment, information on the process of laser desorption of negative ions is obtained. It has been possible to measure the internal energy of a laser-desorbed negative molecular ion for the first time. From our measurements, as well as from theory, we find strong support for a thermal desorption mechanism. Future work will explore other vibrational transitions so that not only the rotational but also the vibrational temperature of the desorbed C_2^- molecule can be identified as has been done for the desorption of neutral C_2 molecules [9].

Acknowledgement

This work was supported by the US Department of Energy, BES-Materials Sciences, under Contract W-31-109-ENG-38.

References

[1] H.J. Heinen, Intern. J. Mass Spectrom. Ion Processes 38 (1981) 309.
[2] D.M. Lubman, ed., Lasers and mass spectrometry (Oxford Univ. Press, New York, 1990).
[3] K.R. Lykke, P. Wurz, D.H. Parker and M.J. Pellin, Appl. Opt. 32 (1993) 857.
[4] N. Fuerstenau, F. Hillenkamp and R. Nitsche, Intern. J. Mass Spectrom. Ion Processes 31 (1979) 85.
[5] G. Seifert, S. Becker and H.J. Dietze, Intern. J. Mass Spectrom. Ion Processes 84 (1988) 121.
[6] P. Wurz, K.R. Lykke, M.J. Pellin, D.M. Gruen and D.H. Parker, Vacuum 43 (1992) 381.
[7] H. Cronberg, M. Reichling, E. Broberg, H.B. Nielsen, E. Mathias and N. Tolk, Appl. Phys. B 52 (1991) 155.
[8] B. Danielzik, N. Fabricius, M. Roewekamp and D. von der Linde, Appl. Phys. Letters 48 (1986) 212.
[9] R.W. Dreyfus, R. Kelly and R.E. Walkup, Nucl. Instr. Meth. B 23 (1987) 557.
[10] J.P. Cowin, D.J. Auerbach, C. Becker and L. Wharton, Surface Sci. 78 (1978) 545.
[11] W. Weltner Jr. and R.J. van Zee, Chem. Rev. 89 (1989) 1713.
[12] K.M. Ervin and W.C. Lineberger, J. Phys. Chem. 95 (1991) 1167.
[13] G. Herzberg and A. Lagerqvist, Can. J. Phys. 46 (1968) 2363.
[14] W.S. Cathro and J.C. Mackie, J. Chem. Soc. Faraday Trans. I 2 (1973) 237.
[15] W.C. Lineberger and T.A. Patterson, Chem. Phys. Letters 13 (1972) 40.
[16] J.E. Hunt, K.R. Lykke and M.J. Pellin, in: Methods and mechanisms for producing ions from large molecules, eds. K.G. Standing and W. Ens (Plenum Press, New York, 1991) p. 309.
[17] M.G. Littman, Appl. Opt. 23 (1984) 4465.
[18] T.D. Raymond, P. Esherick and A.V. Smith, Opt. Letters 14 (1989) 1116.
[19] H. Schomburg, H.F. Doebele and B. Rueckle, Appl. Phys. B 30 (1983) 131.
[20] P. Wurz and K.R. Lykke, J. Phys. Chem. 96 (1993) 10129.
[21] M.A. Schildbach, R.J. Tench, M. Balooch and W.J. Siekhaus, Mat. Res. Soc. Symp. Proc. 191 (1990) 79.
[22] K.P. Huber and G. Herzberg, Constants of diatomic molecules, Vol. 6 (Van Nostrand Reinhold, New York, 1979).

[23] J.F. Ready, in: Effects of high-power laser radiation (Academic Press, New York, 1971) p. 67.
[24] R. Kelly and R.W. Dreyfus, Nucl. Instr. Meth. B 32 (1988) 341.
[25] B.M. Smirnov, Negative ions (McGraw-Hill, New York, 1982).
[26] M.B. Sowa, P.A. Hintz and S.L. Anderson, J. Chem. Phys. 95 (1991) 4719.
[27] P.G. Strupp, J.L. Grant, P.C. Stair and E. Weitz, J. Vacuum Sci. Technol. A 6 (1988) 839.
[28] J.T. Lin and T.F. George, J. Appl. Phys. 54 (1983) 382.
[29] K.R. Spangenberg, Vacuum tubes (McGraw-Hill, New York, 1948).
[30] K.S. Krishnan and S.C. Jain, Nature 169 (1952) 702.
[31] R.F. Willis, B. Feuerbacher and B. Fitton, Phys. Rev. B 4 (1971) 2442.
[32] H. Kawano and F.M. Page, Intern. J. Mass Spectrom. Ion Processes 50 (1983) 1.
[33] H. Hotop and W.C. Lineberger, J. Phys. Chem. Ref. Data 14 (1985) 731.
[34] S. Yang, K.J. Taylor, M.J. Craycraft, J. Conceicao, C.L. Pettiette, O. Cheshnovsky and R.E. Smalley, Chem. Phys. Letters 144 (1988) 431.
[35] K. Raghavachari and J.S. Binkley, J. Chem. Phys. 87 (1987) 2191.
[36] H.R. Leider, O.H. Krikorian and D.A. Young, Carbon 11 (1973) 555.
[37] S.B.H. Bach and J.R. Eyler, J. Chem. Phys. 92 (1990) 358.
[38] P.A. Redhead, Vacuum 12 (1962) 203.